NANO LETTERS

2005
Vol. 5, No. 3
429−434

Liquid Crystalline Nanowires in Porous Alumina: Geometric Confinement versus Influence of Pore Walls

Martin Steinhart,*,† Sven Zimmermann,‡ Petra Göring,† Andreas K. Schaper,§ Ulrich Gösele,† Christoph Weder,|| and Joachim H. Wendorff‡

Max Planck Institute of Microstructure Physics, Weinberg 2, D-6120 Halle, Germany, Institute of Physical Chemistry, Philipps-University, Hans-Meerwein-Strasse, D-35032 Marburg, Germany, Center of Materials Science, Philipps-University, Hans-Meerwein-Strasse, D-35032 Marburg, Germany, and Department of Macromolecular Science and Engineering, Case Western Reserve University, 2100 Adelbert Road, Cleveland, Ohio 44106-7202

Received November 4, 2004; Revised Manuscript Received December 13, 2004

ABSTRACT

Aligned liquid crystalline nanowires within ordered porous alumina templates show a pronounced texture on a macroscopic scale. We have investigated the influence of the geometric confinement and the nature of the pore walls on the mesophase formation by means of X-ray diffraction. The apparent texture is the result of a complex interplay of the pore geometry, interfacial phenomena, and the thermal history. Pores with a diameter of a few hundred nm guide the mesophase formation more efficiently than those with a diameter below 100 nm.

The development of nanoscaled one-dimensional (1D) building blocks for miniaturized devices has emerged as a new and important activity in materials science.[1,2] As a result, nanowires and nanotubes based on a plethora of materials[1−6] have found their way into applications that range from displays and magnetic media[7] to the separation of racemic mixtures,[8] to selective ion transport,[9] to sensors.[10] Martin et al. have pioneered a versatile approach for their fabrication based on the use of porous matrices as molds.[1] Wetting meso- and macroporous templates having pore walls with a high surface energy is a simple methodology to prepare such 1D nanoobjects.[6,11,12] Ordered porous alumina templates[13−15] are characterized by regularly arranged, parallel pores with sharp diameter distribution and uniform pore depth. Nanowire arrays prepared by employing such materials as a mold may exhibit high regularity and specific macroscopic orientation over large areas (order of cm^2). It is obvious that the internal fine structure[16−18] of 1D nanoobjects thus produced largely determines their properties. The question of how the one-dimensional geometric confinement and the nature of the pore walls influence the morphology of the "molded" material, particularly in case of systems characterized by mesoscopic length scales or exhibiting intrinsic anisotropy, has remained largely unanswered.

Here we report on the preparation and morphological characterization of nanowires formed by wetting ordered porous alumina with melts of the liquid crystalline (LC) 2-adamantanoyl-3,6,7,10,11-penta(1-butoxy)triphenylene (Ada-PBT, Figure 1a),[19] a discotic triphenylene derivative. Ada-PBT is representative of an important class of disk-shaped molecules, which spontaneously assemble into columns (Figure 1b). Materials with this structural feature exhibit an extraordinarily high mobility of both charge carriers and optical excitations along the columnar direction.[20−22] The phase behavior of Ada-PBT is as follows:[19] below 75 °C, glassy; above 75 °C, Col_{hp} (hexagonally plastic columnar mesophase); above 168 °C, Col_{ho} (hexagonally ordered columnar mesophase); above 188 °C, isotropic. Both the Col_{hp} and Col_{ho} mesophases are characterized by a hexagonal arrangement of the columns (Figure 1b). In contrast to the Col_{ho} phase the Col_{hp} phase exhibits a correlation between individual columns in the columnar direction, and it differs from a crystalline phase only in the ability of the columns to rotate around their long axes. Earlier investigations on triphenylenes confined to the sponge-like pores of disordered nano- and mesoporous glasses revealed that the formation of the Col_{hp} phase is suppressed under these conditions. Instead, X-ray diffraction (XRD) evidenced the presence of a randomly oriented Col_{ho} phase, even at room temperature.[23]

* Corresponding author. E-mail: steinhart@mpi-halle.de.
† Max Planck Institute of Microstructure Physics.
‡ Institute of Physical Chemistry, Philipps-University.
§ Material Sciences Center, Philipps-University.
|| Case Western Reserve University.

10.1021/nl0481728 CCC: $30.25 © 2005 American Chemical Society
Published on Web 12/31/2004

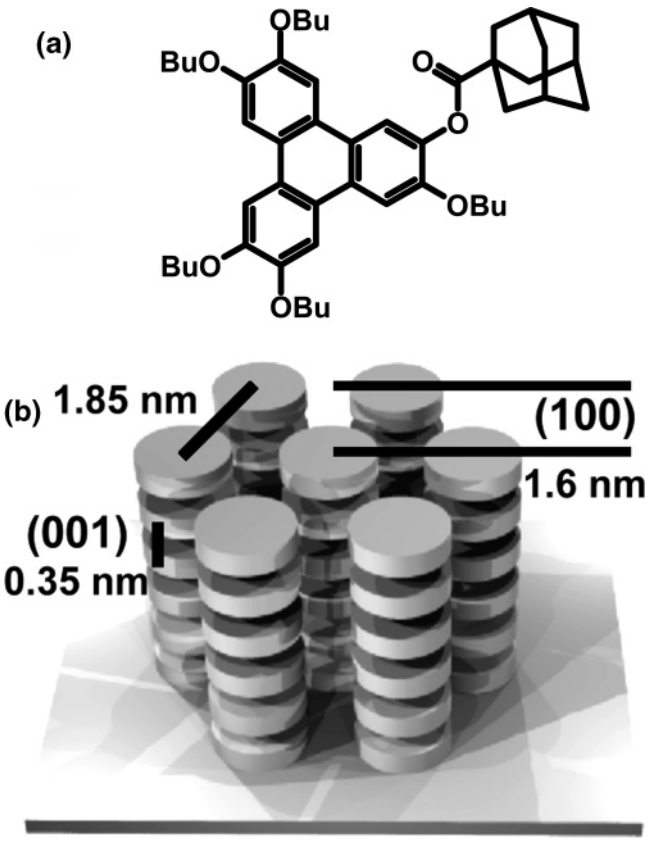

Figure 1. (a) Chemical structure of 2-adamantanoyl-3,6,7,10,11-penta(1-butoxy)triphenylene (Ada-PBT). (b) Schematic representation of columns formed by the disk-shaped Ada-PBT molecules. The lattice plane distance corresponding to the (100) reflection, the resulting intercolumnar distance, and the intracolumnar disk−disk distance corresponding to the (001) reflection are denoted.

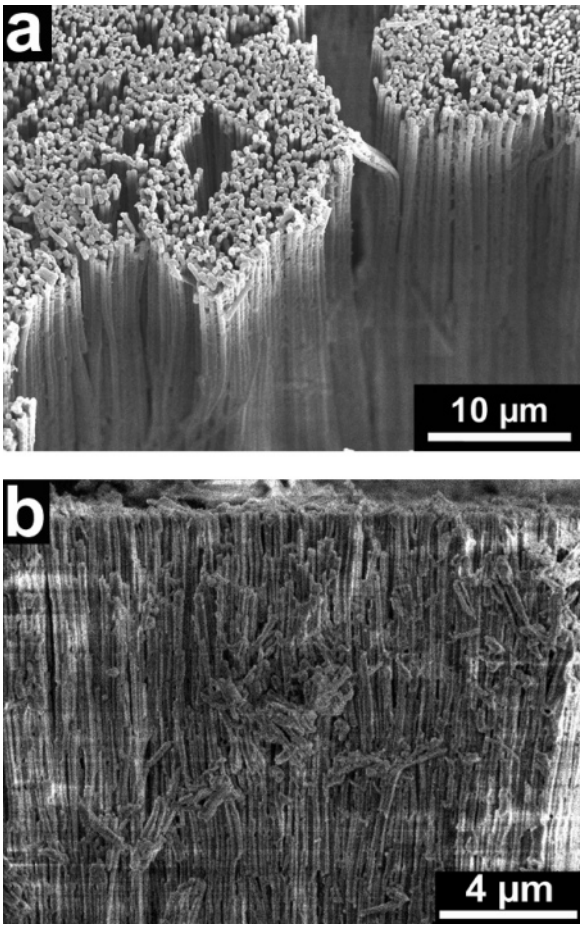

Figure 2. Scanning electron microscopy images of released, aligned Ada-PBT wires with diameters of (a) 400 nm and (b) 60 nm.

The XRD pattern of Ada-PBT[24,25] is characterized by two dominant reflections: the narrow (100) peak at $2\Theta = 5.3°$ ($d = 1.6$ nm) of both the Col_{ho} and the Col_{hp} phase, corresponding to an intercolumnar center-to-center distance of 1.85 nm, and the weaker peak at 25.5° ($d = 0.35$ nm) (Figure 1b). The latter reflection represents the intracolumnar disk−disk distance and is indexed as (001) for the Col_{ho} phase.

It is highly desirable to combine the specific properties of functional materials such as Ada-PBT with the advantages of 1D nanostructures. Indeed, Ada-PBT nanowires can be easily prepared by infiltrating porous alumina templates at a temperature at which the Ada-PBT is in the isotropic liquid state. Figure 2 shows arrays of aligned Ada-PBT nanowires thus produced after selectively etching the templates with aqueous KOH (20 wt-%). The nanowires exhibit diameters of 400 and 60 nm, respectively, and perfectly reflect the dimensions of the templates employed.

The intrinsic supramolecular architecture of the Ada-PBT nanowires determines their properties to a high degree. For many applications, ensembles of aligned nanowires are required, which exhibit uniaxial arrangement of the columns on a macroscopic scale. The realization of such a texture has proven exceedingly difficult to achieve in thin film configurations.[26−28] There are two distinct orientations of the columnar axes relative to an interface: normal (homeotropic) and parallel (planar). One may expect that the columns predominantly grow parallel to the long axis of a confining 1D pore, i.e., planar with respect to the pore walls. Moreover, it seems to be trivial that the guidance of the mesophase formation by the pore geometry becomes more efficient when the pore diameter is decreased.

It is, however, well-known that the interactions between triphenylenes and a substrate on which they have been deposited strongly influence the ordering of the columns in a way that depends on the nature of the substrate.[29−31] Often, a homeotropic orientation is preferred. This is obvious from Figure 3a, which represents a $\Theta/2\Theta$ scan of an approximately 500 μm thick Ada-PBT film (all XRD experiments were performed in reflection mode with a Philips X'pert MRD diffractometer with a cradle and secondary monochromator for Cu Kα radiation). The sample was prepared by melting the Ada-PBT on a silicon wafer covered by a native oxide layer at 208 °C and quickly (<5 s) quenching the material to room temperature by rapidly immersing it into water. The $\Theta/2\Theta$ scan of the Ada-PBT film thus produced shows the characteristic feature of the Col_{ho} phase, that is, the single intracolumnar (001) peak at $2\Theta = 25.4°$. It is striking that this peak has an extremely high intensity, whereas the intercolumnar (100) peak at $2\Theta = 5.15°$ is very weak. Since only homeotropically oriented columns can contribute to the intensity of the intracolumnar, and only planar oriented ones

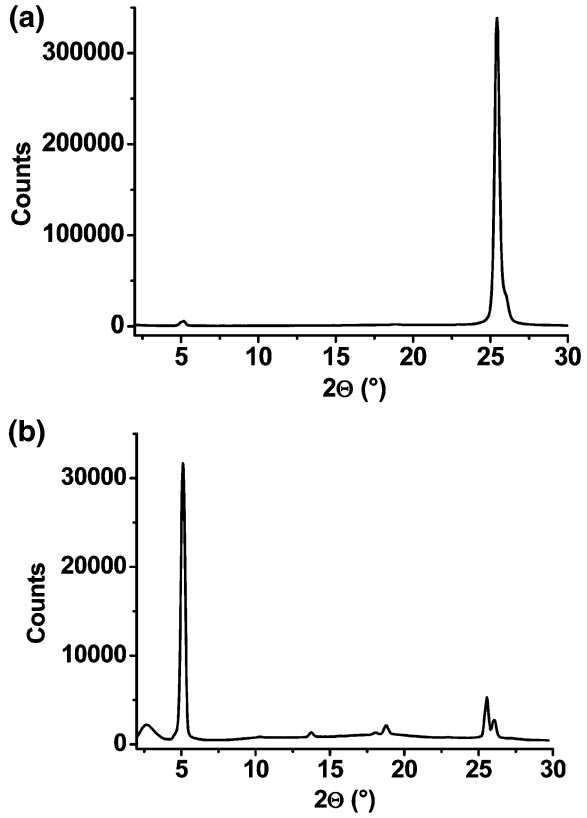

Figure 3. XRD pattern of bulk Ada-PBT. (a) Θ/2Θ-Scan of a thick film on a silicon wafer rapidly quenched from the melt and (b) typical powder pattern of Ada-PBT.

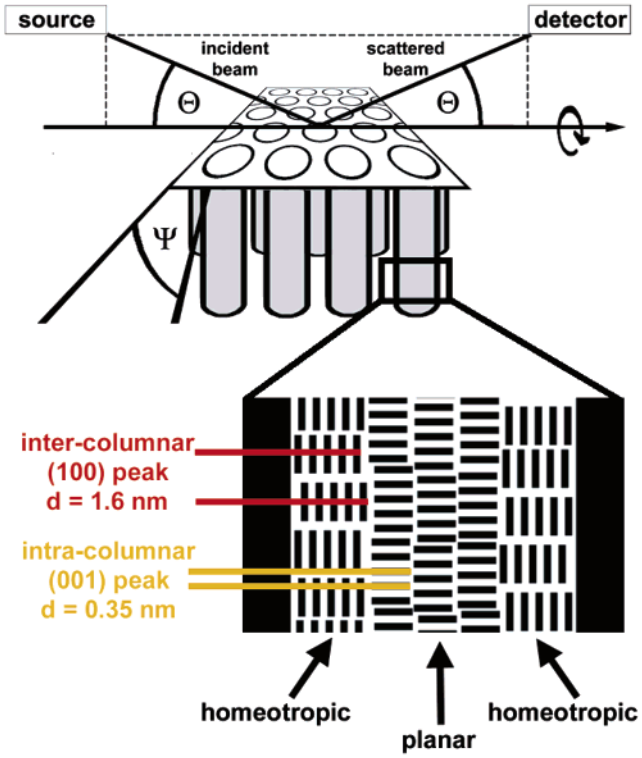

Figure 4. Schematic representation of the XRD setup. For the Θ/2Θ scans the samples were placed in the device so that the surface of the template was oriented perpendicularly to the plane of incident and scattered X-ray beams. In this geometry the intercolumnar (100) reflection (d = 1.6 nm) originates from the columns oriented homeotropically with respect to the pore walls, the intracolumnar (001) peak (d = 0.35 nm) from those oriented parallel to the long axes of the pores. For the Ψ-scans, the setup was adjusted to selected 2Θ angles. The samples were tilted by an angle Ψ around an axis defined by the intersection of the template surface and the plane of the incident and the scattered X-ray beams.

to the intensity of the intercolumnar peak, the XRD pattern evidences a rather uniaxial, homeotropic orientation of the columns on a macroscopic scale over the entire film thickness, whereas a negligible proportion of the columns exhibit a planar orientation. This suggests that the growth of the columns starts off from molecules whose molecular plane is parallel to the wafer surface. This simple experiment demonstrates that interfaces in contact with the liquid crystal have a crucial influence on the mesophase formation. Figure 3b shows for comparison a typical powder diffractogram of bulk Ada-PBT consisting of the Col_{hp} phase, as it is indicated by the occurrence of the characteristic double peak[24,25] at 2Θ = 25.6° and 2Θ = 26°. A very important feature is that the intercolumnar (100) peak has a much higher intensity than the intracolumnar reflection at 25.6°; the intensity ratio is approximately 7:1.

If Ada-PBT nanowires are formed using porous alumina as a mold, the geometry of the pores should promote an alignment of the columns parallel to their long axes. On the other hand, the Ada-PBT/pore wall interactions may act competitively since it is to be expected that the LC molecules in contact with the walls prefer an orientation where their molecular plane is parallel to the interface. We melted Ada-PBT on the surface of ordered porous alumina with pore diameters D_p of 400 and 60 nm and pore depths of 100 μm. A cylindrical pore segment with a height of 1 nm has a wall surface of 1257 nm^2 and a volume of 125663 nm^3 for D_p = 400 nm, and a wall surface of 189 nm^2 and a volume of 2827 nm^3 for D_p = 60 nm. Thus, the surface-to-volume ratio increases by nearly 1 order of magnitude if D_p is decreased from 400 to 60 nm. Templates with D_p values of 400 and 60 nm were first heated to 208 °C, infiltrated with Ada-PBT, and subsequently quenched by rapid immersion into water. A second series of samples was prepared by melting the Ada-PBT on the template surface at 200 °C for 15 min under an argon atmosphere. After applying a vacuum the specimens were cooled to 70 °C, where Ada-PBT is in its glassy state, at rates of 0.9, 0.17, and 0.017 K/min, respectively. Then we mechanically removed the residual material on the template surface with a sharp blade and selectively etched away the aluminum substrate on which the porous alumina layer was located using a mixture of 1.7 g $CuCl_2 \cdot H_2O$, 50 mL concentrated HCl and 50 mL deionized water. The sample was placed in the diffractometer in such a way that the pore bottoms were turned up so that predominantly material within the pores contributed to the scattered intensity. In this geometry the aligned nanowires within the template were oriented parallel to the plane defined by the incident X-ray beam and the detector (Figure 4). Therefore, only the columns oriented parallel to the long axes of the pores contribute to the intensity of the intracolumnar (001) peak, and vice versa the ones oriented perpendicularly to the long axes of the pores to the intercolumnar (100)

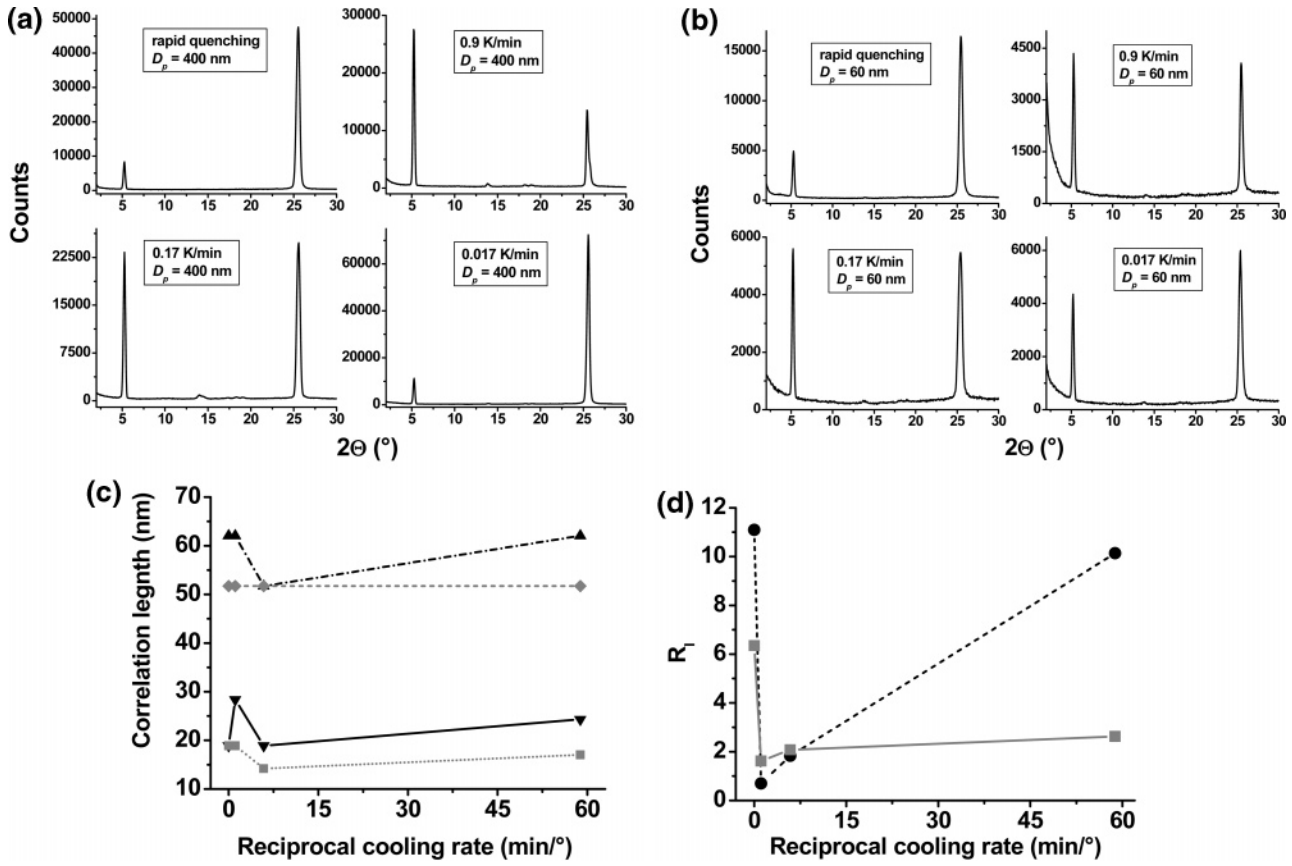

Figure 5. Θ/2Θ scans on Ada-PBT wires aligned within the template pores cooled from the melt to the glassy state at different rates. (a) $D_p = 400$ nm; (b) $D_p = 60$ nm. (c) Correlation lengths versus the reciprocal cooling rate: black up-pointing triangles, intercolumnar (100) peak, $D_p = 400$ nm; gray diamonds, intercolumnar (100) peak, $D_p = 60$ nm; black down-pointing triangles, intracolumnar (001) peak, $D_p = 400$ nm; gray squares, intracolumnar (001) peak, $D_p = 60$ nm. (d) R_I as a function of the reciprocal cooling rate. Black circles, $D_p = 400$ nm, gray squares, $D_p = 60$ nm.

reflection. Changes of the intensity ratio between the two peaks thus indicate corresponding changes of the proportion of columns that have adapted one of these distinct orientations.

Figure 5a shows the Θ/2Θ scans measured on the 400 nm samples and Figure 5b the corresponding XRD patterns of the 60 nm samples. As expected, all the samples consisted of the Col_{ho} phase and showed a pronounced texture. The relative intensity of the intracolumnar (001) reflection, in comparison to that of the intercolumnar (100) reflection, was for every sample investigated much stronger than in case of the corresponding powder pattern. Thus, the columns are predominantly arranged parallel the long axes of the template pores, i.e., planar with respect to the pore walls. The correlation lengths ascribed to the intracolumnar (001) peak by means of the Debye−Scherrer method[32] were in the range of 14 to 18 nm in case of the 60 nm and 18 to 28 nm in case of the 400 nm samples. The correlation lengths calculated from the fwhm values of the intercolumnar (100) peak amounted to approximately 50 nm for the 60 nm and 60 nm for the 400 nm samples (Figure 5c). The overall tendency is, thus, that the degree of intrinsic order of the mesophase is slightly higher within 400 nm pores. The striking result, however, is the strong dependence of the intensity ratio of the intra- and the intercolumnar peaks $R_I = I_{(001)}/I_{(100)}$ on both the thermal history and the pore diameter. Figure 5d represents R_I as a function of the reciprocal cooling rate. In case of the quickly quenched samples, R_I amounts to 11.1 for $D_p = 400$ nm and 6.4 for $D_p = 60$ nm. This evidences a rapid growth of the columns parallel to the long axes of the pores, which is, however, increasingly disturbed as the surface-to-volume ratio increases with diminishing pore diameter. R_I decreases to below 2 at a cooling rate of 0.9 K/min, indicating that the relative proportion of columns arranged homeotropically with respect to the pore walls has increased. These molecular stacks obviously emanate from the pore walls and grow toward the pore centers. Thereby, the proportion of columns oriented parallel to the long axes of the pores is reduced. The value of R_I for the 400 nm pores (0.7) is smaller than that for the 60 nm pores (1.6). The most plausible reason for this finding is that the stronger curvature of the smaller pores disturbs the growth of the homeotropic columns. Surprisingly, a reversal in the structure formation process was observed at a slower cooling rate of 0.17 K/min: R_I is 1.8 for $D_p = 400$ nm and 2.0 for $D_p = 60$ nm. When the cooling rate is further reduced by 1 order of magnitude to 0.017 K/min, R_I increases only slightly to 2.6 for $D_p = 60$ nm, but significantly to 10.1 for $D_p = 400$ nm, a value that is comparable to that of the rapidly quenched sample. This finding evidences the crucial role of the pore diameter. We speculate that the phase oriented homeotropically with respect to the pore walls is

characterized by an equilibrium correlation length in the columnar direction, leaving a considerably larger proportion of the columns aligned with the long axes of the pores with $D_p = 400$ nm. This correlation length, however, cannot be determined with the XRD setup used here. If an uniaxial arrangement of the columns in the nanowires is desired, the guiding efficiency of the larger pores 400 nm in diameter is more pronounced than that of the 60 nm pores.

To further investigate the texture of the Ada-PBT nanowires we performed Ψ scans on all the samples. The settings of Θ (incident beam) and 2Θ (detector) were fixed to values corresponding to the maximum intensity of the intercolumnar (100) and intracolumnar (001) peaks. The samples were tilted by an angle Ψ around the axis defined by the intersection of the plane of the incident and the scattered X-ray beams with the template surface (Figure 4). The scattering intensity is measured as a function of the tilting angle Ψ with an increment of 1° and an integration time of 20 s. The Ψ curves thus directly represent the orientational distribution of the columns. However, the sensitivity of the setup used here steeply decreases at Ψ values larger than 70°, and for Ψ = 90° virtually no intensity is detectable, independent of the nature of the sample. The corresponding curves for D_p = 400 nm are represented in Figure 6a, and for $D_p = 60$ nm in Figure 6b, respectively. In all cases the orientational distribution of the columns parallel to the pore axes is rather narrow. The fwhm of the curves measured at 2Θ values corresponding to the maximum intensity of the intracolumnar (001) reflection amounts to values between 6° and 7° for D_p = 400 nm, and 8° to 9° for $D_p = 60$ nm. The fwhm of the Ψ scans belonging to the intercolumnar (100) reflection lie between 25° and 28° for $D_p = 400$ nm, and between 25° and 31° for $D_p = 60$ nm, with a minimum at a cooling rate of 0.9 K/min, where the relative intensity of the intercolumnar reflection and thus the extent of homeotropic orientation has a maximum. We assume that a phase of well-ordered columns aligned with the long axes of the pores exists in their cores, whereas the homeotropic phase emanates from the pore walls, forming a shell that surrounds the core phase. We interpret the relative broadness of the orientational distribution of the homeotropic phase as a signature of the presence of a transition layer between the two orientational states of order. The thickness of this layer should be determined by the curvature elastic properties of the Ada-PBT. An indication supporting this model is that the orientational distribution is relatively narrow as the overall amount of the homeotropic phase is high, because then the proportion of "undisturbed" and thus highly ordered homeotropic areas is relatively large. Again, the tendency is that the orientation of the columns is more pronounced within the 400 nm pores. Further investigations on the thermal properties of the Ada-PBT wires by means of differential scanning calorimetry are in progress.

In conclusion, we have fabricated aligned nanowires of a discotic model compound using ordered porous alumina templates. The LC columns are highly oriented along the long axes of the template pores, but LC/pore wall interactions counteract and promote the growth of columns having a homeotropic orientation with respect to the pore walls. It is highly desirable to fabricate LC nanowires exhibiting a strong texture and thus high mobility of both charge carriers and optical excitations along their long axes. An efficient direction of the mesophase formation requires, however, the

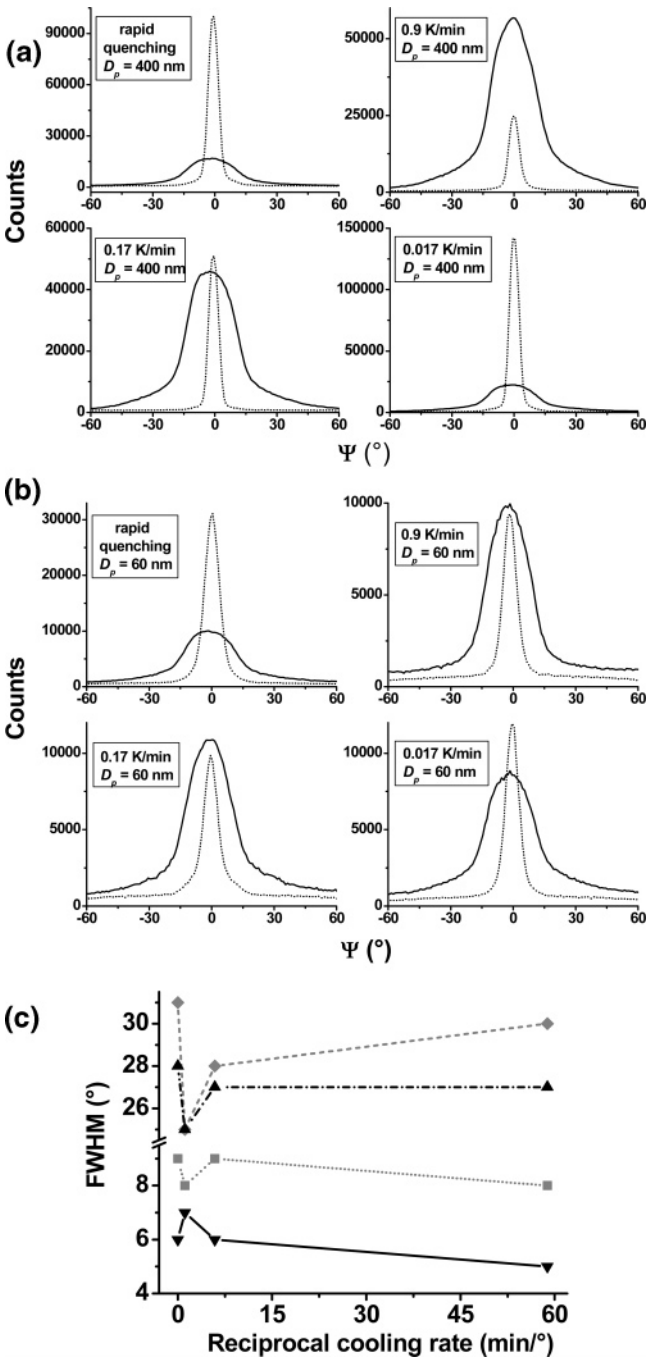

Figure 6. Ψ-scans on Ada-PBT wires aligned within the template pores cooled from the melt to the glassy state at different rates. Solid curves, 2Θ value corresponds to intensity maximum of the intercolumnar (100) reflection; dotted curves, 2Θ value corresponds to intensity maximum of the intracolumnar (001) reflection. (a) D_p = 400 nm; (b) $D_p = 60$ nm; (c) fwhm of the Ψ-scans plotted versus the reciprocal cooling rate. Black up-pointing triangles, intercolumnar (100) peak, $D_p = 400$ nm; gray diamonds, intercolumnar (100) peak, $D_p = 60$ nm; black down-pointing triangles, intracolumnar (001) peak, $D_p = 400$ nm; gray squares, intracolumnar (001) peak, $D_p = 60$ nm.

optimization of the thermal history and the surface-to-volume ratio of the pores. In case of our model system the use of pores with $D_p = 400$ nm yielded nanowires with a higher degree of orientational and intrinsic columnar order than the use of pores with a diameter of 60 nm. These results may have significant impact on the design of 1D building blocks of materials characterized by mesoscopic length scales or intrinsic anisotropy. Particularly the chemical modification of the pore walls, that is, tuning their polarity, could allow for a precisely controlled generation of one-dimensional supramolecular architectures.

Acknowledgment. The authors thank Silko Grimm for the preparation of the templates. S.Z. acknowledges financial support by the Studienstiftung des Deutschen Volkes.

References

(1) Martin, C. R. *Science* **1994**, *266*, 1961−1966.
(2) Huang, Y.; Duan, X. F.; Cui, Y.; Lauhon, L. J.; Kim, K. H.; Lieber, C. M. *Science*, **2001**, *294*, 1313−1317.
(3) Schnur, J. M. *Science* **1993**, *262*, 1669−1676.
(4) Evans, E.; Bowman, H.; Leung, A.; Needham, D.; Tirrell, D. *Science* **1996**, *273*, 933−935.
(5) Bognitzki, M.; Hou, H. Q.; Ishaque, M.; Frese, T.; Hellwig, M.; Schwarte, C.; Schaper, A.; Wendorff, J. H.; Greiner, A. *Adv. Mater.* **2000**, *12*, 637−640.
(6) Steinhart, M.; Wendorff, J. H.; Greiner, A.; Wehrspohn, R. B.; Nielsch, K.; Schilling, J.; Choi, J.; Gösele, U. *Science* **2002**, *296*, 1997.
(7) Kovtyukhova, N. I.; Mallouk, T. E.; Mayer, T. S. *Adv. Mater.* **2003**, *15*, 780−785.
(8) Lee, S. B.; Mitchell, D. T.; Trofin, L.; Nevanen, T. K.; Soderlund, H.; Martin, C. R. *Science* **2002**, *296*, 2198−2200.
(9) Nishizawa, M.; Menon, V. P.; Martin, C. R. *Science* **1995**, *268*, 700−702.
(10) Steinle, E. D.; Mitchell, D. T.; Wirtz, M.; Lee, S. B.; Young, V. Y.; Martin, C. R. *Anal. Chem.* **2002**, *74*, 2416−2422.
(11) Steinhart, M.; Wendorff, J. H.; Wehrspohn, R. B. *ChemPhysChem* **2003**, *4*, 1171−1176.
(12) Steinhart, M.; Wehrspohn, R. B.; Gösele, U.; Wendorff, J. H. *Angew. Chem., Int. Ed.* **2004**, 1334−1344.
(13) Masuda, H.; Fukuda, K. *Science* **1995**, *268*, 1466−1468.
(14) Masuda, H.; Yada K.; Osaka, A. *Jpn. J. Appl. Phys., Part 2* **1998**, *37*, L1340−L1342.
(15) Nielsch, K.; Choi, J.; Schwirn, K.; Wehrspohn, R. B.; Gösele U. *Nano Lett.* **2002**, *2*, 677−680.
(16) Steinhart, M.; Senz, S.; Wehrspohn, R. B.; Gösele, U.; Wendorff, J. H. *Macromolecules* **2003**, *36*, 3646−3651.
(17) Steinhart, M.; Jia, Z.; Schaper, A.; Wehrspohn, R. B.; Gösele, U.; Wendorff, J. H. *Adv. Mater.* **2003**, *15*, 706−709.
(18) Luo, Y.; Lee, S. K.; Hofmeister, H.; Steinhart, M.; Gösele, U. *Nano Lett.* **2004**, *4*, 143−147.
(19) Bayer, A.; Kopitzke, J.; Noll, F.; Seifert, A.; Wendorff, J. H. *Macromolecules* **2001**, *34*, 3600−3606.
(20) Adam, D.; Schuhmacher, P.; Simmerer, J.; Häusslinger, L.; Siemensmeyer, K.; Etzbach, K. H.; Ringsdorf, H.; Haarer, D. *Nature* **1994**, *371*, 141−143.
(21) Simmerer, J.; Glüsen, B.; Paulus, W.; Kettner, A.; Schuhmacher, P.; Adam, D.; Etzbach, K. H.; Siemensmeyer, K.; Wendorff, J. H.; Ringsdorf, H.; Haarer, D. *Adv. Mater.* **1996**, *8*, 815−819.
(22) Marguet, S.; Markovitsi, D.; Millie, P.; Sigal, H.; Kumar, S. *J. Phys. Chem. B* **1998**, *102*, 4697−4710.
(23) Kopitzke, J.; Wendorff, J. H.; Glüsen, B. *Liq. Cryst.* **2000**, *27*, 643−648.
(24) Glüsen, B.; Kettner, A.; Wendorff, J. H. *Mol. Cryst. Liq. Cryst.* **1997**, *303*, 115−120.
(25) Kettner, A.; Wendorff, J. H. *Liq. Cryst.* **1999**, *26*, 483−487.
(26) Kevenhörster, B.; Kopitzke, J.; Seifert, A. M.; Tsukruk, V.; Wendorff, J. H. *Adv. Mater.* **1999**, *11*, 246−250.
(27) Zimmermann, S.; Wendorff, J. H.; Weder, C. *Chem. Mater.* **2002**, *14*, 2218−2223.
(28) Tracz, A.; Jeszka, J. K.; Watson, M. D.; Pisula, W.; Müllen, K.; Pakula, T. *J. Am. Chem. Soc.* **2003**, *125*, 1682−1683.
(29) Wegner, H.; Weiss, K.; Grunze, M.; Wöll, C. *Appl. Phys. A* **1997**, *65*, 231−234.
(30) Hurt, R.; Krammer, G.; Crawford, G.; Jian, K. Q.; Rulison, C. *Chem. Mater.* **2002**, *14*, 4558−4565.
(31) Piris, J.; Debije, M. G.; Stutzmann, N.; van de Craats, A. M.; Watson, M. D.; Müllen, K.; Warman, J. M. *Adv. Mater.* **2003**, *15*, 1736−1740.
(32) Guinier, A. *X-ray Diffraction*, 2nd ed.; Dover Publications: Mineola, 1994.

NL0481728